FRANCK–CONDON DOMINATED CHEMISTRY. FORMATION AND DISSOCIATIONS OF THE DIMETHYLHYDROXYSULFURANYL RADICAL

František TUREČEK

Department of Chemistry, Bagley Hall, Box 351700, University of Washington, Seattle, WA 98195-1700, U.S.A.; e-mail: turecek@chem.washington.edu

Received February 2, 2000
Accepted February 25, 2000

Dedicated to Professor Otakar Červinka on the occasion of his 75th birthday.

The structure and energetics of the hydroxyl radical adduct to dimethyl sulfide (DMS) was revisited using high level *ab initio* calculations. Density functional theory B3LYP/6-31++G(2d,p) and perturbational MP2(FULL)/6-31++G(2d,p) calculations found a weakly bound structure, $(CH_3)_2SOH^{\bullet}$, with a long S–O bond that was a local energy minimum. Single point calculations at the effective QCISD(T)/6-311++G(3df,2p) level of theory, denoted as G2++(MP2), found the $(CH_3)_2S$–$OH^{\bullet}$ bonding energy to be 40 kJ mol^{-1} at 298 K. The standard heat of formation of $(CH_3)_2SOH^{\bullet}$ was assessed from dissociation and isodesmic reactions as –45 ± 4 kJ mol^{-1}. No other local minima corresponding to C_2H_7OS radicals were found at the present level of theory that could be derived from DMS or dimethyl sulfoxide (DMSO). A very weak complex, $CH_3S(H)$–$^{\bullet}OCH_3$, was found that was bound by mere 4 kJ mol^{-1} against dissociation to CH_3SH and $^{\bullet}OCH_3$. Vertical electron capture by $(CH_3)_2SOH^+$ is predicted to form $(CH_3)_2SOH^{\bullet}$ with a highly non-relaxed geometry corresponding to a vibrational excitation of 138 kJ mol^{-1} above the local minimum and 88 kJ mol^{-1} above the dissociation threshold to DMS and $OH^{\bullet}$. Unimolecular dissociation of $(CH_3)_2SOH^{\bullet}$ to methanesulfenic acid (CH_3SOH) and $CH_3^{\bullet}$ faces an energy barrier that diminishes at shorter S–O distances. The dipole-allowed electronic excitation in $(CH_3)_2SOH^{\bullet}$ was calculated with CIS/6-311++G(2df,p) to have λ_{max} = 248 nm in the gas phase. The resulting *B* state represents a charge-transfer complex of $(CH_3)_2S^{+\bullet}$ and OH^-. The present computational results allowed us to explain the existing controversy between the experimental results obtained by gas-phase flow kinetics, radiolysis in aqueous solution, and neutralization-reionization mass spectrometry.

Key words: *Ab initio* calculations; Dimethyl sulfide; Dimethyl sulfoxide; Oxidations; Radicals; Gas-phase chemistry; Mass spectrometry; Atmospheric chemistry.

The atmospheric oxidation of dimethyl sulfide (DMS) has been of considerable interest to chemists and atmospheric scientists for about three decades[1]. The diurnal tropospheric chemistry of DMS consists mainly of the reaction with hydroxyl radical that triggers an oxidation cascade resulting

in the eventual formation of sulfuric and methanesulfonic acid[2]. In spite of the substantial flux of DMS into the troposphere which is estimated at $4–4.5 \cdot 10^7$ tons/year (ref.[3]), the equilibrium concentrations of DMS (ref.[3]) and OH$^\bullet$ (ref.[4]) in the marine biolayer are too low to permit *in situ* studies of DMS oxidation. The mechanism of the reaction between DMS and OH radical has been the subject of numerous recent studies. Laboratory studies used gas-phase flow reactors[5,6] to generate OH$^\bullet$ radicals by pulse-photolysis of water[5] or hydrogen peroxide[7]. The kinetics of the OH$^\bullet$ reaction with DMS was monitored as the rate of OH$^\bullet$ depletion under pseudo first-order conditions of large excess of DMS in the system. These studies found that the kinetics of OH$^\bullet$ depletion differed in the presence and absence of molecular oxygen. From a combination of kinetic studies, two mechanisms were suggested as shown in Scheme 1. Path (i) corresponds to hydrogen atom abstraction from DMS by OH$^\bullet$. Reaction (i) was calculated to be 105 kJ mol^{-1} exothermic[8] and showed a small activation barrier that was measured at 1.1–2 kJ mol^{-1} (refs[5,9]). Reaction (ii) corresponds to the formation of a $(CH_3)_2SOH^\bullet$ adduct that reacts with molecular oxygen to form OOH$^\bullet$ and, presumably, dimethyl sulfoxide[10–13] (DMSO). From kinetic analysis that was based on the rate of disappearance of OH$^\bullet$, it was concluded that $(CH_3)_2SOH^\bullet$ was a bound species (an intermediate), and the dissociation energy of the S–O bond was estimated as 54 ± 13 kJ mol^{-1} (ref.[7]), which was later revised to 45 ± 10 kJ mol^{-1} (ref.[10]).

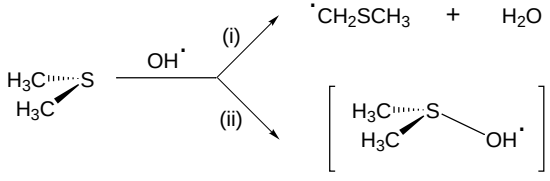

SCHEME 1

An attempt at direct generation of $(CH_3)_2SOH^\bullet$ in the gas phase has been made using collisional electron transfer to the stable $(CH_3)_2SOH^+$ cation, corresponding to O-protonated DMSO (Scheme 2)[14]. $(CH_3)_2SOH^\bullet$ formed by femtosecond reduction of $(CH_3)_2SOH^+$ was found to be unstable on the time scale of the measurements (4.2 μs) and dissociated completely to form competitively methanesulfenic acid and DMS that were detected directly by mass spectrometry. This result was supported by Hartree–Fock level *ab initio* calculations with the 6-31G(d) basis set that predicted that $(CH_3)_2SOH^\bullet$ was unbound[14].

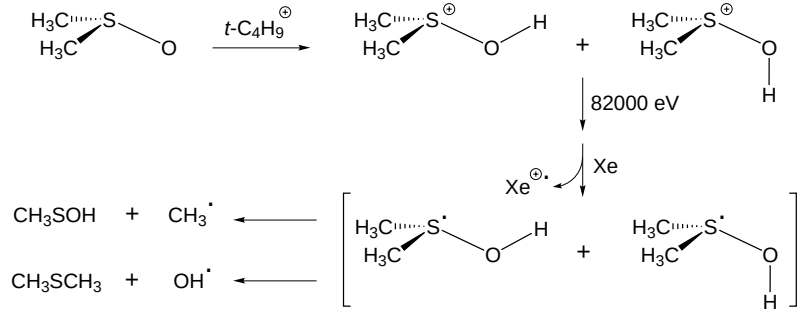

SCHEME 2

Computational studies of $(CH_3)_2SOH^\bullet$ stability yielded different results[8,15]. McKee used Møller–Plesset perturbational theory, MP2(frozen core), with the 6-31+G(2d) basis set to conclude that $(CH_3)_2SOH^\bullet$ was a bound structure possessing a long S–O bond[15]. The dissociation energy of the S–O bond was obtained from approximated single-point QCISD(T)/6-31+G(2d,p) calculations as 25 kJ mol^{-1}, which was somewhat lower than the then current estimate[10] (54 kJ mol^{-1}). Tureček used MP2(FULL)/6-31+G(d) calculations to obtain a dipole–dipole complex of DMS with $OH^\bullet$ that did not involve an S–O bond and was bound by 17 kJ mol^{-1} against dissociation to DMS and $OH^\bullet$, when calculated at the MP4(SDQ)/6-31+G(d) level of theory[8].

In parallel with gas-phase studies, $(CH_3)_2SOH^\bullet$ radical and higher homologues have been long considered as transient intermediates of the oxidation of sulfides with radiolytically produced OH radicals in aqueous solution. The experimental evidence for the transient intermediacy of $(CH_3)_2SOH^\bullet$ followed from the UV-VIS spectra of DMS solutions, saturated with N_2O and irradiated with 4.6 MeV electrons[16]. The transient formation of $(CH_3)_2SOH^\bullet$ was deduced from an absorption band at λ_{max} = 358 nm (refs[17–19]). An additional evidence for a transient intermediate was provided by electron-spin resonance[20] and conductivity studies[17,21].

In view of the different conclusions reached by previous calculations[8,15], it appeared of interest to re-examine the structure and energetics of the $(CH_3)_2SOH^\bullet$ radical at a level of theory sufficiently high to provide definite data. The present paper addresses the following points: (i) Examine the equilibrium structure of $(CH_3)_2SOH^\bullet$ using perturbational *ab initio* and density functional theory. (ii) Obtain high-quality thermochemical data for $(CH_3)_2SOH^\bullet$, its dissociations and bimolecular reactions with triplet dioxygen. (iii) Explain the gas-phase dissociations of $(CH_3)_2SOH^\bullet$ formed by femtosecond collisional electron transfer. We show that the unimolecular

gas-phase dissociations are governed by large Franck–Condon effects in the formation of $(CH_3)_2SOH^{\bullet}$.

CALCULATIONS

Standard *ab initio* calculations were performed using the Gaussian 98 suite of programs[22]. Geometries were optimized with density functional theory (DFT) calculations[23] using Becke's hybrid functional (B3LYP)[24,25] and the 6-31++G(2d,p) basis set. The latter is a split-valence basis set of double-ζ quality furnished with two shells of d functions on C, O, and S, one shell of p functions on H, and diffuse functions on all atoms[26]. Previous studies showed that geometry optimizations at this level of theory of sulfur molecules, radicals, and cations provided reliable structures[27,28]. The structure of $(CH_3)_2SOH^{\bullet}$ radical was also optimized with Møller–Plesset theory[29] truncated at second order, MP2(FULL), using the 6-31++G(2d,p) basis set. Reaction paths in $(CH_3)_2SOH^{\bullet}$ were investigated with B3LYP/6-31++G(2d,p) calculations in which one or two internal coordinates were fixed while the remaining internal degrees of freedom were fully optimized. Spin unrestricted formalisms were used for calculations of open-shell species. The B3LYP optimized geometries were characterized by harmonic frequency calculations as local minima (all frequencies real). MP2(FULL) frequencies were not calculated because they required very large disk space for systems of this size. The B3LYP frequencies were scaled by 0.963 (for the various scaling factors used for DFT frequencies see refs[30–33]) and used to calculate zero-point energy corrections, vibrational enthalpies and entropies. $(CH_3)_2SOH^{\bullet}$, DMS, CH_3SOH, and DMSO have several low frequency modes corresponding to methyl torsions about the C–S bonds and the hydroxyl torsion about the S–O bond. The methyl torsions in DMS (175 and 176 cm^{-1}), DMSO (175 and 218 cm^{-1}), CH_3SOH (178 cm^{-1}), and $(CH_3)_2SOH^{\bullet}$ (157, 170, and 175 cm^{-1}), and the OH torsion in $(CH_3)_2SOH^{\bullet}$ (68 cm^{-1}, all corrected wavenumbers) were treated as free rotors. Previous studies have shown that this treatment introduces only small errors when compared with the more rigorous hindered rotor analysis[34–36]. The remaining vibrations were treated using the rigid rotor-harmonic oscillator approximation.

Single point energies were obtained on the B3LYP or MP2(FULL) optimized geometries by expanding the basis set to 6-311++G(2df,p), 6-311++G(3df,2p), and the much larger correlation-consistent basis set aug-cc-pVTZ (ref.[37]). In addition, single-point energies were calculated with quadratic configuration interaction including single, double and extrapo-

lated triple excitations[38] (QCISD(T)) and used for composite energies defined in Eq. (*1*):

$$\text{QCISD(T)/6-311++G(3df,2p)} \approx \text{QCISD(T)/6-31++G(d,p)} + \quad (1)$$
$$+ \text{ MP2/6-311++G(3df,2p)} - \text{MP2/6-31++G(d,p)} .$$

This basis set expansion is analogous to the Gaussian 2 (MP2) scheme[39], and its various modifications[40–43], and it has been used previously for accurate calculations of energies of hypervalent sulfur radicals[44]. By analogy with G2(MP2), we denote the scheme in Eq. (*1*) as G2++(MP2) with the provision that it does not include empirical corrections for the number of valence electrons[39] and the zero-point energy corrections are introduced in calculations of relative energies. The reason for using the G2++(MP2) scheme instead of the usual and computationally similar G2(MP2) scheme was dictated by the electronic nature of the radicals in question. The G2(MP2) scheme incorporates a QCISD(T) single-point calculation with a split valence triple-ζ basis set to account for energies of strongly bound electrons, but omits diffuse functions, which are introduced only through a basis set expansion. In this way weak, long range interactions which are typical for hypervalent radicals are neglected in the pivotal QCISD(T) calculation. The G2++(MP2) scheme, which includes diffuse functions on all atoms in all single-point calculations, puts more emphasis on the treatment of long range interactions which are important for the energetics of hypervalent radicals and other loosely bound species.

The bond dissociation energies did not show any diminishing trends when calculated with the valence triple-ζ and the much larger aug-cc-pVTZ basis set. It was therefore deemed that basis set superposition effects were negligible at this level of theory and counterpoise corrections were not implemented in the relative energy calculations.

Spin contamination in unrestricted B3LYP calculations was negligible as judged by the $\langle S^2 \rangle$ expectation values that were within 0.75–0.76 for doublets and 2.00–2.01 for triplets. Spin contamination in UMP2 calculations was also small and resulted in $\langle S^2 \rangle$ expectation values that were within 0.75–0.79 for doublets and 2.00–2.05 for triplets. The spin contamination was partially corrected by Schlegel's annihilation procedure[45,46] that lowered the total energies by <4.2 millihartree (root mean square deviation, rmsd). The G2++(MP2) energies were much less sensitive to spin contamination because of cancellation of errors in the MP2 terms. The UMP2 and

PMP2 based energies differed by <0.5 millihartree (1.3 kJ mol^{-1}) rmsd. In addition to spin-unrestricted MP2 calculations, we also obtained energies using the restricted-open shell formalism, ROMP2 (ref.[47]). It has been suggested recently that ROMP2 calculations with moderately large basis sets can provide good quality radical stabilization energies for systems encumbered with spin contamination problems[48].

RESULTS AND DISCUSSION

Structure and Energetics of $(CH_3)_2SOH^{\cdot}$ Radical

Geometry optimizations with both B3LYP/6-31++G(2d,p) and MP2(FULL)/6-31++G(2d,p) resulted in a local minimum for the $(CH_3)_2SOH^{\bullet}$ radical (Fig. 1). The MP2(FULL) geometry was in a good agreement with that obtained previously by McKee at a slightly lower level of theory[15]. In particular, the S–O and S–C bonds and the C–S–C, C–S–O, and H–O–S bond angles agreed well with those reported previously[15]. It appears that extending the basis set to 6-31++G(2d,p) and using excitation of all electrons in the MP2 treatment did not have a critical effect on the quality of the optimized geometries. However, the equilibrium geometries obtained by B3LYP and MP2(FULL) somewhat differed (Table I). In particular, B3LYP predicted an S–O bond and S–C bonds than were 0.277 and 0.017 Å longer, respectively, than those from the MP2(FULL) optimization. This result was qualitatively consistent with geometry optimizations of the analogous $(CH_3)_2S^{\bullet}$–SH radical for which B3LYP gave an S–S bond that was 0.084 Å longer than that from MP2 optimization with

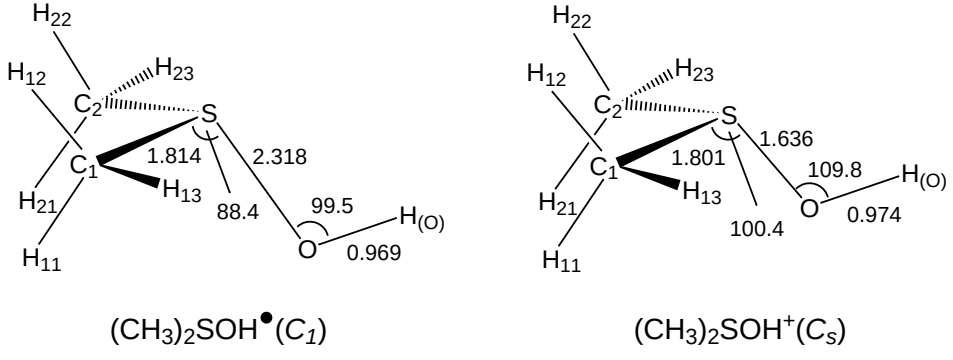

FIG. 1
B3LYP/6-31++G(2d,p) optimized geometries of $(CH_3)_2SOH^{\cdot}$ and $(CH_3)_2SOH^{+}$. For other geometry parameters see Table I

TABLE I
Optimized geometries of $(CH_3)_2SOH^{\bullet}$ radical[a]

Bond	B3LYP/ 6-31++G(2d,p)	MP2(FULL)/ 6-31++G(2d,p)	Angle	B3LYP/ 6-31++G(2d,p)	MP2(FULL)/ 6-31++G(2d,p)	Dihedral angle	B3LYP/ 6-31++G(2d,p)	MP2(FULL)/ 6-31++G(2d,p)
C1–S	1.814	1.797	C1–S–C2	100.5	99.5	O–S–C1–C2	87.9	88.3
C2–S	1.814	1.797	O–S–C1	88.4	88.4	H(O)–O–S–C1	130.0	131.0
O–S	2.318	2.041	O–S–C2	88.3	88.6	H11–C1–S–C2	62.3	64.9
H(O)–O	0.969	0.966	H(O)–O–S	99.5	104.2	H12–C1–S–C2	–60.5	–57.5
H11–C1	1.093	1.088	H11–C1–S	110.2	109.9	H13–C1–S–C2	181.5	–175.3
H12–C1	1.091	1.086	H12–C1–S	108.7	107.9	H21–C2–S–C1	–61.6	–64.8
H13–C1	1.092	1.086	H13–C1–S	106.9	107.3	H22–C2–S–C1	61.2	57.6
H21–C2	1.093	1.088	H21–C2–S	110.2	110.0	H23–C2–S–C1	179.3	175.4
H22–C2	1.091	1.086	H22–C2–S	108.7	107.9			
H23–C2	1.092	1.086	H23–C2–S	106.9	107.3			

[a] Bond lengths in Å, bond and dihedral angles in °.

the same basis set[44]. However, for the isomeric $CH_3S–S^{\bullet}(H)CH_3$ radical, MP2 yielded a longer S–S bond than did B3LYP, so there does not appear to be a general trend in radical geometries optimized by these two methods[44]. Regardless of the different geometries, both B3LYP and MP2 predicted a long S–O bond in $(CH_3)_2SOH^{\bullet}$ indicating a low bond dissociation energy. To account for the differences in the optimized geometries of $(CH_3)_2SOH^{\bullet}$, single-point energies were calculated for sets of B3LYP and MP2(FULL) geometries for all species involved.

The $(CH_3)_2S\cdots HO^{\bullet}$ dipole–dipole complex found previously[8] has also been reexamined by MP2(FULL) and B3LYP geometry optimizations with the 6-31++G(2d,p) basis set. In contrast to the previous finding that has been reproduced in the present work, calculations with the larger basis set found no local energy minimum for a dipole–dipole complex. Hence, the existence of a dipole–dipole complex is not supported at the present level of theory and was likely an artifact of optimizations with the smaller basis set used previously.

Do other isomers of $(CH_3)_2SOH^{\bullet}$ exist? We used the structures of stable $C_2H_7OS^+$ isomers[28] as starting points to investigate possible radical candidates. Of those, $CH_3SO^{\bullet}(H)CH_3$ and $CH_3S^{\bullet}(H)OCH_3$ are hypervalent oxonium and sulfonium radicals, respectively, that are known to be marginally stable or unstable in ground electronic states[49–52]. Attempted geometry optimizations with B3LYP and MP2(FULL) of $CH_3S–O^{\bullet}(H)CH_3$ resulted in a dissociation of the S–O bond and formation of a loose van der Waals complex of $CH_3S^{\bullet}$ and CH_3OH. The S–O distance in the $CH_3S^{\bullet}\cdots CH_3OH$ complex (3.37 Å by B3LYP) indicated no chemical bonding between S and O, which was further corroborated by electron distribution that showed the spin density to be entirely localized in the CH_3S moiety. Geometry optimizations of $CH_3S^{\bullet}(H)OCH_3$ yielded a local potential energy minimum (Fig. 2). The S–O bond lengths differed for B3LYP and MP2(FULL) optimized structures, 2.774 and 2.056 Å, respectively. Atomic spin densities in $CH_3S(H)–^{\bullet}OCH_3$, *e.g.* 0.75 at O and 0.16 at S, showed partial spin density transfer from the methoxy radical to the methanethiol moiety that indicated weak bonding. The G2++(MP2) single-point energies based on the B3LYP geometries showed that $CH_3SH–^{\bullet}OCH_3$ was 34–36 kJ mol^{-1} less stable than $(CH_3)_2SOH^{\bullet}$. However, $CH_3SH–^{\bullet}OCH_3$ was only very weakly bound with respect to dissociation to CH_3SH and $CH_3O^{\bullet}$ as judged by the 298 K bond dissociation energy that was only 4 kJ mol^{-1} by G2++(MP2). Interestingly, single-point energies obtained for the seemingly tighter MP2(FULL) structure showed substantial destabilization and predicted exothermic dis-

sociation to CH_3SH and $CH_3O^{\bullet}$. It can be concluded from the present calculations that a complex of methanethiol with the methoxy radical is extremely weakly bound and does not involve a regular chemical bond between S and O.

No intrinsic stability was also expected for complexes of H_2O with the CH_3SCH_2 radical, in part because the two-electron bonding in the corresponding cations was already relatively weak (40–44 kJ mol^{-1})[28]. Note that the CH_3SCH_2–$O^{\bullet}H_2$ structure is a hypervalent oxonium radical, while $CH_3S(OH_2)CH_2^{\bullet}$ would involve a four electron interaction between S and O which can be expected to be non-bonding. We also investigated computationally the *S,S*-dimethyl-*S*-oxo-*S*-hydrosulfuranyl radical, $(CH_3)_2S(H)$–$O^{\bullet}$ that corresponds to a product of one-electron reduction of a stable ion structure[28]. However, attempted geometry optimizations with B3LYP/6-31++G(2d,p) resulted in a dissociation of the S–H bond to produce DMSO and a hydrogen atom. Hence, the existence of bound *S,S*-dimethyl-*S*-oxo-*S*-hydrosulfuranyl radical is not supported at the present level of theory.

Important for the present study is the comparison of the optimized structures of $(CH_3)_2SOH^{\bullet}$ and its ion precursor, *anti*-$(CH_3)_2SOH^+$ (ref.[28]). The differences between the ion and radical structures are highlighted in Fig. 1. The ion shows a substantially shorter S–O bond, shorter C–S bonds, and

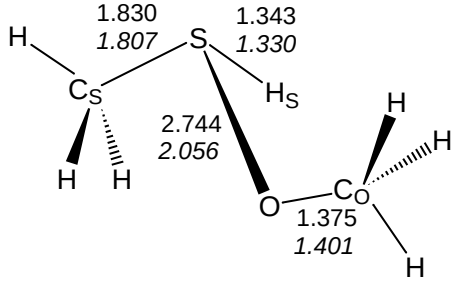

O-S-C_S = 83.6, *84.5*
H-S-C_S = 97.2, *98.3*
C_O-O-S = 112.3, *109.8*
C_O-O-S-C_S = 140.9, *170.0*
O-S-C_S-H_S = 68.1, *88.7*

FIG. 2
Optimized structure of $CH_3S(H)$–$^{\bullet}OCH_3$. B3LYP/6-31++G(2d,p) geometry parameters are shown as roman numerals, MP2(FULL)/6-31++G(2d,p) values are shown as italics. Bond lengths in Å, bond and dihedral angles in °

larger C–S–O and S–O–H angles than does the radical. Hence, vertical electron transfer to $(CH_3)_2SOH^+$ can be expected to be accompanied by Franck–Condon effects.

The thermochemistry of $(CH_3)_2SOH^\bullet$ radical was investigated at the G2++(MP2) level of theory by evaluating standard enthalpies for reactions (*2*)–(*5*) ($\Delta H_{rxn,298}$). To assess the effects of the different optimized structures of $(CH_3)_2SOH^\bullet$ and also the effect of spin-contamination in calculations of open-shell species, reaction enthalpies were calculated for six sets of G2++(MP2) total energies corresponding to UB3LYP and UMP2(FULL) optimized geometries and UMP2, PMP2, and ROMP2 single-point energies used in Eq. (*1*). The complete set of calculated energies is given in Table II. Equations (*2*)–(*5*) summarize the enthalpies obtained from G2++(PMP2) calculations that showed the smallest standard deviation in the calculated $\Delta H_{f,298}$ of $(CH_3)_2SOH^\bullet$.

$$(CH_3)_2SOH^\bullet \longrightarrow DMS + OH^\bullet \qquad (2)$$

$$\Delta H_{rxn,298} = 40.0 \text{ kJ mol}^{-1}$$
$$\Delta H_{f,298} = -38.5 \text{ kJ mol}^{-1}$$

$$(CH_3)_2SOH^\bullet \longrightarrow DMSO + H^\bullet \qquad (3)$$

$$\Delta H_{rxn,298} = 114.1 \text{ kJ mol}^{-1}$$
$$\Delta H_{f,298} = -46.6 \text{ kJ mol}^{-1}$$

$$(CH_3)_2SOH^\bullet \longrightarrow CH_3SOH + CH_3^\bullet \qquad (4)$$

$$\Delta H_{rxn,298} = 52.4 \text{ kJ mol}^{-1}$$
$$\Delta H_{f,298} = -48.6 \text{ kJ mol}^{-1}$$

$$(CH_3)_2SOH^\bullet + (^3\Sigma_u)O_2 \longrightarrow DMSO + OOH^\bullet \qquad (5)$$

$$\Delta H_{rxn,298} = -83.8 \text{ kJ mol}^{-1}$$
$$\Delta H_{f,298} = -45.8 \text{ kJ mol}^{-1}$$

$$(CH_3)_2SOH^\bullet + (^3\Sigma_u)O_2 \longrightarrow CH_3SOH + CH_3OO^\bullet \qquad (6)$$

$$\Delta H_{rxn,298} = -81.7 \text{ kJ mol}^{-1}$$

Reaction enthalpies in Eqs (*2*)–(*4*) are the dissociation energies for the S–O, O–H, and S–C bonds in $(CH_3)_2SOH^{\bullet}$. Equations (*5*) and (*6*) are isodesmic reactions for hydrogen atom and methyl transfer, respectively. When combined with the pertinent enthalpies of formation of DMS (–37.5 ± 2 kJ mol^{-1})[53], DMSO (–150.5 ± 1.5 kJ mol^{-1})[53], $OH^{\bullet}$ (–37.5 ± 2 kJ mol^{-1})[53], $OOH^{\bullet}$ (20.9 kJ mol^{-1})[53,54], CH_3SOH (–141.8 kJ mol^{-1})[8], $CH_3^{\bullet}$ (145.7 kJ mol^{-1})[53], and $H^{\bullet}$ (218 kJ mol^{-1})[53], one obtains the standard enthalpies of formation for $(CH_3)_2SOH^{\bullet}$ as shown

TABLE II
Reaction enthalpies[a] for reactions (*2*)–(*6*)

Method	$\Delta H_{rxn,298}$[b], kJ mol^{-1}				
	reaction (*2*)	reaction (*3*)	reaction (*4*)	reaction (*5*)	reaction (*6*)
B3LYP/6-31++G(2d,p)[c]	53	166	64	–38	–61
B3LYP/6-311++G(2df,p)[c]	54	146	55	–55	–69
B3LYP/aug-cc-pVTZ[c]	51	157	53	–48	–71
PMP2/6-311++G(3df,2p)[c]	29	71	28	–77	–62
ROMP2/6-311++G(3df,2p)[c]	20	58	20	–55	–40
PMP2/aug-cc-pVTZ[c]	28	91	29	–64	–64
ROMP2/aug-cc-pVTZ[c]	20	79	21	–42	–42
QCISDT/6-311++G(3df,2p)// B3LYP/6-31++G(2d,p)[c,d]					
UMP2	39	112	51	–86	–84
PMP2	40	114	52	–84	–82
ROMP2	38	112	50	–83	–81
QCISDT/6-311++G(3df,2p)// UMP2(FULL)/6-31++G(2d,p)[e]					
UMP2	36	109	48	–92	–88
PMP2	38	111	51	–88	–85
ROMP2	41	114	53	–82	–79

[a] Corresponding reactions see the text. [b] At 298 K. [c] Based on B3LYP/6-31++G(2d,p) optimized geometries, zero-point, and enthalpy corrections. [d] Effective energies from Eq. (*1*). [e] Effective energies from Eq. (*1*) based on UMP2(FULL)/6-31++G(2d,p) optimized geometries and B3LYP/6-31++G(2d,p) zero-point and enthalpy corrections.

in Eqs (*2*)–(*5*). Reaction (*6*) could not be evaluated because of lack of an experimental enthalpy of formation for the methylperoxy radical[53]. The mean enthalpy of formation from Eqs (*2*)–(*5*) is $\Delta H_{f,298}$ [$(CH_3)_2SOH^{\bullet}$] = –45 ± 4 kJ mol^{-1} which does not include the uncertainties in the experimental enthalpies of formation. Evaluation of Eqs (*2*)–(*5*) with G2++(UMP2) and G2++(ROMP2) energies gave $\Delta H_{f,298}$ [$(CH_3)_2SOH^{\bullet}$] = –43 ± 4 and –44 ± 5 kJ mol^{-1}, respectively, which were practically indistinguishable. The G2++(MP2) reaction enthalpies that were based on MP2(FULL) optimized geometries are summarized in Table II. The corresponding $\Delta H_{f,298}$ [$(CH_3)_2SOH^{\bullet}$] were –39 ± 4, –42 ± 5, and –46 ± 5 kJ mol^{-1} for the UMP2, PMP2, and ROMP2 single-point calculations, respectively. The spread in the $\Delta H_{f,298}$ [$(CH_3)_2SOH^{\bullet}$] values was somewhat greater when based on the MP2(FULL) geometries, but still within the usual accuracy target of the composite G2 procedures[39–41].

In contrast, B3LYP energies obtained with both the 6-311++G(2df,p) and aug-cc-pVTZ basis sets deviated from those obtained by G2++(MP2) calculations. For example, the B3LYP/aug-cc-pVTZ reaction enthalpies were 51, 157, 53, and –48 kJ mol^{-1} for reactions (*2*)–(*5*), respectively (Table II), showing good agreement only for reaction (*4*). Consequently, the enthalpy of formation for $(CH_3)_2SOH^{\bullet}$ calculated by B3LYP (–67 ± 21 kJ mol^{-1}) differed from the G2++(MP2) datum, and also showed an unacceptably large spread depending on the reaction used. It can be concluded that even when large basis sets are used, B3LYP does not provide reliable thermochemistry for $(CH_3)_2SOH^{\bullet}$ radical. It is worth noting in this context that G2++(MP2) gave a correct reaction enthalpy for the dissociation $OOH^{\bullet} \rightarrow (^3\Sigma_u)O_2 + H^{\bullet}$ ($\Delta H_{rxn,298}$ = 197.8 kJ mol^{-1}) compared with the experimental value (198.1 kJ mol^{-1}), and B3LYP/aug-cc-pVTZ also performed well ($\Delta H_{rxn,298}$ = 202 kJ mol^{-1}). However, the occasional and perhaps fortuitous agreement of B3LYP relative energies with experimental or high-quality computational data for some systems cannot be safely extrapolated to other systems.

The strength of the S–O bond in $(CH_3)_2SOH^{\bullet}$ was previously estimated from kinetic data as 45 ± 10 kJ mol^{-1} (ref.[10]) The G2++(MP2) reaction enthalpy reported here (40 kJ mol^{-1}, Eq. (*2*)) is somewhat smaller, although it falls within the error limits that were reported for the previous estimates. On the basis of the calculated $\Delta H_{f,298}$, the datum from reaction (*2*) is somewhat lower than those from reactions (*3*)–(*5*). An upward correction by one standard deviation of the $\Delta H_{f,298}$ values would bring the calculated S–O bond dissociation energy in $(CH_3)_2SOH^{\bullet}$ in perfect agreement with the estimate from kinetic measurements.

The effective QCISD(T)/6-31+G(2d,p) calculation of McKee gave a weaker bond, $\Delta H_{rxn,0}$ = 25 kJ mol^{-1} at 0 K corresponding to $\Delta H_{rxn,298}$ = 28 kJ mol^{-1} at 298 K. The difference between the present and previous results is due to the basis set expansion in the effective QCISD(T)/6-311++G(3df,2p) energies. The present QCISD(T)/6-31++G(d,p) single-point calculations gave $\Delta H_{rxn,0}$ = 28 kJ mol^{-1} at 0 K, consistent with McKee's results.

Reactions (*5*) and (*6*) were previously evaluated by Barone *et al.*[11] who reported $\Delta H_{rxn,298}$ = –95 kJ mol^{-1} for both reactions at an unspecified temperature. The present calculations indicate that the reactions with triplet dioxygen are less exothermic than thought previously.

The G2++(MP2) bonding energies (reaction (*2*)) were further used for Gibbs energy calculations. To calculate reaction entropies, the methyl torsions in $(CH_3)_2SOH^{\bullet}$ and DMS were treated as vibrations, while the S–OH torsion was treated as a free rotation. The former simplifying assumption was based on the similarity between the reduced moments of inertia for CH_3–S rotations in DMS and $(CH_3)_2SOH^{\bullet}$ on one hand, and the similar wavenumbers for the methyl torsions in DMS and $(CH_3)_2SOH^{\bullet}$ on the other. The entropy terms corresponding to these internal degrees of freedom largely canceled out regardless of whether the latter were treated as vibrations of free rotations. Regarding the free rotation of the hydroxyl group in $(CH_3)_2SOH^{\bullet}$, the barrier for the hydroxyl rotation was estimated from Eq. (*7*) (ref.[55]),

$$V_0 = 2I_{red}(2\pi\nu)^2/r^2, \qquad (7)$$

where I_{red} is the reduced moment of inertia, ν is the torsional frequency (68 cm^{-1} or 0.8 kJ mol^{-1}), and r is the rotation degeneracy taken as 1. The estimated barrier, 1.9 kJ mol^{-1}, was substantially smaller than the vibrational enthalpy of $(CH_3)_2SOH^{\bullet}$ (10.3 kJ mol^{-1} at 298 K), indicating nearly free rotation of the hydroxyl group at room temperature. According to the detailed analysis by East and Radom, use of the free-rotor approximation can be recommended for rotational barriers lower than 1.4*RT* or 2.3–3.5 kJ mol^{-1} at 200–298 K (ref.[36]).

The calculated ΔG_{rxn} and equilibrium constants (K_{eq}) for the gas-phase dissociation of $(CH_3)_2SOH^{\bullet}$ to DMS and $OH^{\bullet}$ are shown in Table III. The data show that OH and DMS engage in a weak complex. At the DMS concentrations used in the previous experiments (2.5–12.0)·10^{12} molecule cm^{-3} (refs[10,11]), about one in 28 000–135 000 hydroxyl radicals on average will be

bound in a $(CH_3)_2SOH^\bullet$ complex at room temperature. At 250 K, the fraction of $(CH_3)_2SOH^\bullet$ bound $OH^\bullet$ radicals is predicted as one in 1 000–4 800.

Formation of $(CH_3)_2SOH^\bullet$ by Vertical Electron Transfer

The weak bonding between DMS and OH in the $(CH_3)_2SOH^\bullet$ radical strongly suggests that dissociation to DMS and $OH^\bullet$ should be the dominant unimolecular reaction of the $(CH_3)_2SOH^\bullet$ radical. In contrast, $(CH_3)_2SOH^\bullet$ formed by vertical electron transfer showed another major dissociation channel forming CH_3SOH and $CH_3^\bullet$ (ref.[14]). To account for the observed dissociations and the lack of surviving $(CH_3)_2SOH^\bullet$, we investigated computationally the reaction coordinates along the S–O and C–S bonds in $(CH_3)_2SOH^\bullet$. Figure 3 shows the relative energies obtained from single-point B3LYP/6-311++G(2df,p) calculations at several points along the S–O coordinate.

Vertical electron capture in $(CH_3)_2SOH^+$ forms $(CH_3)_2SOH^\bullet$ radical with a highly non-relaxed geometry. In particular, Fig. 1 shows a substantial compression of the S–O bond and a different orientation of the DMS and OH subunits in vertically formed $(CH_3)_2SOH^\bullet$ when compared with the relaxed geometry. A combination of these factors results in a highly elevated potential energy corresponding to vertical landing on the potential energy surface of $(CH_3)_2SOH^\bullet$. The calculated single-point energy of vertically neutral-

TABLE III
Gibbs energies and equilibrium constants for the reaction $(CH_3)_2SOH^\bullet \rightarrow DMS + OH^\bullet$

T, K	ΔG_T, kJ mol^{-1}			K_{eq}, mol l^{-1}		
	G2++(UMP2)	G2++(PMP2)	G2++(ROMP2)	G2++(UMP2)	G2++(PMP2)	G2++(ROMP2)
250	11.2	12.5	10.8	0.004	0.002	0.006
260	10.1	11.4	9.6	0.009	0.005	0.011
270	9.0	10.3	8.5	0.018	0.010	0.022
273.15	8.6	9.9	8.2	0.022	0.013	0.027
280	7.9	9.2	7.4	0.034	0.019	0.042
290	6.7	8.0	6.3	0.061	0.036	0.075
298.15	5.8	7.1	5.3	0.096	0.056	0.116

ized $(CH_3)_2SOH^{\bullet}$ was 138 kJ mol^{-1} above the local minimum and 88 kJ mol^{-1} above the dissociation threshold calculated at the same level of theory. When converted to vibrational energy, this excitation should result in fast dissociation to thermochemically accessible products such as those in reactions (*2*)–(*4*). In contrast, the energy excess alone was insufficient to drive consecutive dissociations of the primary products.

The potential energy surface governing the dynamics of the exothermic dissociations of vertically neutralized $(CH_3)_2SOH^{\bullet}$ was studied by grid calculations in which the S–O bond was fixed and one of the C–S bonds was stretched in steps. The potential energy profile along the S–O coordinate showed steeply decreasing energy as the S–O bond was stretched from 1.636 Å in vertically neutralized $(CH_3)_2SOH^{\bullet}$ to the equilibrium position (Fig. 3). In addition, one of the C–S bond lengths was asymmetrically elongated at the shortest S–O distances. This asymmetric elongation gradually disappeared as the S–O bond was relaxed to reach the equilibrium length. The potential energy surface along the C–S bond was investigated for structures in which the S–O bond was fixed (Fig. 3). This was equivalent to investigating the depth of a gully along a contour on a three-dimensional potential energy hypersurface. At d(S–O) = 1.636 Å, gradual elongation of one of the C–S bonds resulted in potential energy increases that reached a ridge at d(C–S) = 2.15 Å that was 30 kJ mol^{-1} above the bottom of the gully. At longer S–O bond lengths, the gully was deeper, *e.g.*, >50 kJ mol^{-1} at

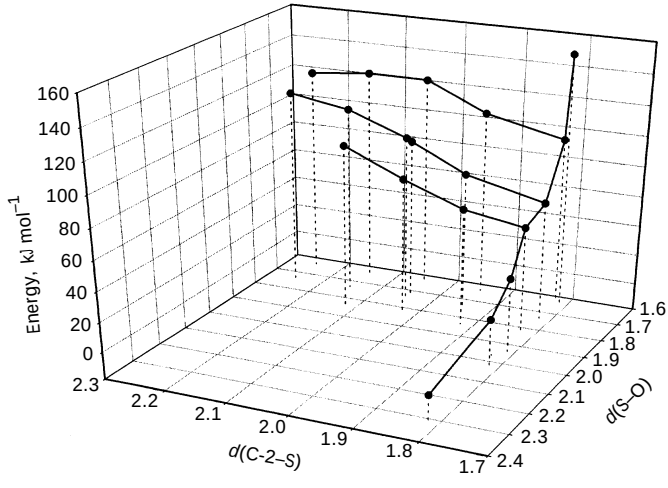

FIG. 3
Potential energy profile along the S–O and S–C bonds in $(CH_3)_2SOH^{\bullet}$

d(S–O) = 1.736 Å, indicating stabilization of the C–S bonds as the S–O bond was gradually relaxed.

This observation was compatible with the nature of chemical bonds in $(CH_3)_2SOH^{\bullet}$. Interaction of the closed-shell electronic system of DMS with the unpaired electron of $OH^{\bullet}$ results in a flow of spin density into the bonding and antibonding orbitals in the DMS moiety. Within the LCAO approximation, this requires mixing of outer shell atomic orbitals on sulfur, oxygen, and carbon to accommodate the unpaired electron. Mulliken population analysis showed the spin density to be mostly shared between the oxygen atom (0.58) and the sulfur atom (0.44) in the equilibrium structure $(CH_3)_2SOH^{\bullet}$ corresponding to the long S–O bond. The single-occupied molecular orbital (SOMO) that accommodates most of the spin density was an antibonding orbital that had nodal surfaces between the S and O atoms (Fig. 4). Upon compressing the S–O bond, the spin density flowed into the long C–S bond such that at the shortest distance, d(S–O) = 1.636 Å, the Mulliken spin densities became 0.59 (S), 0.25 (C), and 0.13 (O). The SOMO in the compressed structure is delocalized among S, the more distant carbon atom, and the oxygen atom. The SOMO nodal properties are such that it is σ-antibonding and π-bonding between S and C as well as between S and O (Fig. 5).

Is the observed C–S bond dissociation compatible with the repulsive nature of the potential energy surface along the S–O coordinate in vertically formed $(CH_3)_2SOH^{\bullet}$? The answer can be found in the effect of the vibrational energy on the geometry of the precursor $(CH_3)_2SOH^{+}$ cation. The precursor cation was formed by gas-phase protonation at 523 K; at this temperature the S–O stretching vibration (767 cm^{-1}, corrected) has a non-negligible population of $n > 0$ states. Using the analytical formula derived by Dunbar[56], we obtained 11% of $n = 1$ and 1.3% of $n = 2$ vibrational states for the S–O stretch in $(CH_3)_2SOH^{+}$ at 523 K. Since in $n > 0$ vibrational states the probability maxima for internuclear distances are close to the vibrational amplitude extremes, $(CH_3)_2SOH^{\bullet}$ radicals formed vertically from the $n = 1$ and $n = 2$ vibrational states of $(CH_3)_2SOH^{+}$ must have bimodal populations of S–O bond distances. This bimodality along the S–O coordinate can be approximated using the potential energy profile expressed by a Morse function (Eq. (*8*))

$$V(x) = D\{1 - \exp[-a(x - x_0)^2]\} , \qquad (8)$$

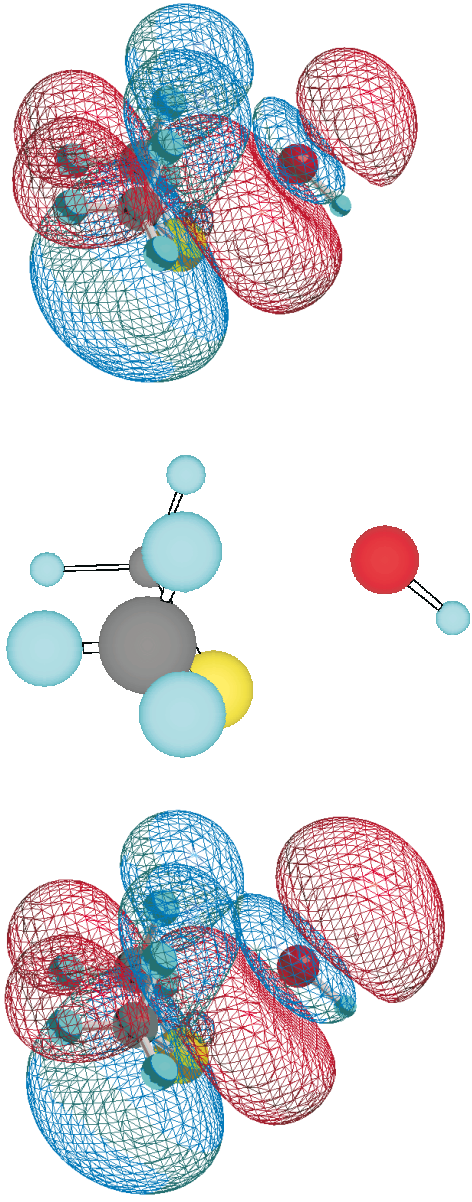

FIG. 4
Single-occupied molecular orbitals (SOMO) in the *B* excited state (top) and *X* ground state (bottom) of optimized $(CH_3)_2SOH^{\bullet}$ from Mulliken populations with the 6-31++G(2d,p) wave function. The long S–O bond is disconnected in the ball-and-stick structure in the middle

where D is the 0 K bond dissociation energy (340 kJ mol^{-1})[28], $a = (k/2D)^{1/2}$, and k is the force constant for the S–O bond stretching vibration in $(CH_3)_2SOH^+$ (4.58 millidyne Å^{-1} or 458 N m^{-1}). Considering the vibrational excitation $n = 0 \rightarrow n = 1$ ($h\nu$ = 9.2 kJ mol^{-1}), the amplitude of the S–O bond vibration ranges between 1.52 and 1.76 Å. Likewise, excitation to $n = 2$ results in S–O bond extremes at 1.47 and 1.81 Å. Since collisional electron transfer takes place in a few femtoseconds while the vibrational period of the S–O stretch is T = 43 fs, the S–O bond in $(CH_3)_2SOH^+$ cannot relax during the electron transfer event, and the $(CH_3)_2SOH^\bullet$ radical is produced with the "instantaneous" geometry of the ion. This simplified analysis suggests that a fraction of $(CH_3)_2SOH^\bullet$ must be produced with S–O bonds compressed to 1.47–1.52 Å. At this distances the potential energy along the S–O coordinate is likely to be highly repulsive. However, the potential energy

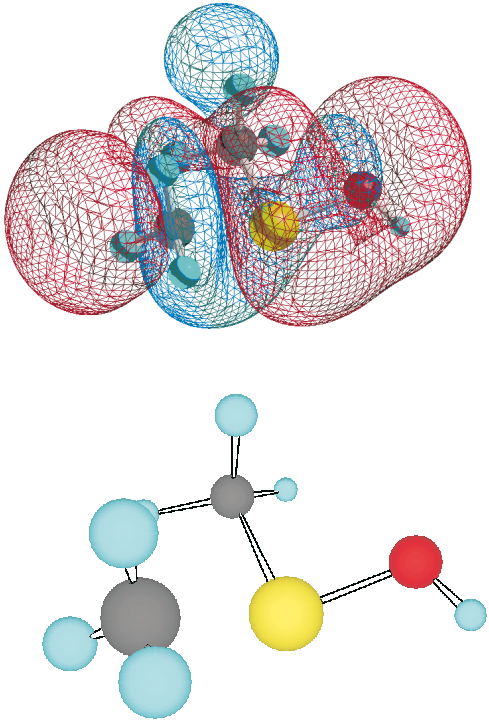

FIG. 5
Single-occupied molecular orbital (SOMO) in $(CH_3)_2SOH^\bullet$ at d(S–O) = 1.636 Å from Mulliken populations with the 6-31++G(2d,p) wave function. The long C–S bond is disconnected in the ball-and-stick structure

surface along the C–S coordinate gets shallower at shorter S–O distances (*vide supra*) and probably becomes repulsive in regions where the S–O bond is very short. In such a case, there will be no dynamic constraints to dissociation of the C–S bond leading to the formation of CH_3SOH and $CH_3^{\bullet}$, in line with the observed dissociations of vertically formed $(CH_3)_2SOH^{\bullet}$ radicals.

We have also addressed the question of excited electronic states in relaxed and vertically formed $(CH_3)_2SOH^{\bullet}$. This was done at a relatively low level of theory using configuration interaction singles[57] (CIS) with the 6-311++G(2df,p) basis set. The excitation energies, wavelengths and oscillator strengths are listed in Table IV. The CI matrices showed substantial configuration mixing, as documented by the absence of a single dominant configuration. The lowest two excitations in relaxed $(CH_3)_2SOH^{\bullet}$ correspond to $n\beta \rightarrow m\beta$ electron transitions. Relaxed $(CH_3)_2SOH^{\bullet}$ showed a single dipole-allowed transition for $X \rightarrow B$ at 248 nm. The calculated wavelength, which pertains to photon absorption in the gas phase, is shorter than that observed for the radiolytically generated $(CH_3)_2SOH^{\bullet}$ radi-

TABLE IV
Excited state energies and oscillator strengths in $(CH_3)_2SOH^{\bullet}$

Species	State	ΔE^a eV	λ_{max} nm	f^b	Major configuration[c]
$(CH_3)_2SOH^{\bullet}$,	$X \rightarrow A$	1.65	752	0.0002	19β→30β(0.57)
relaxed geometry	*B*	5.00	248	0.20	21β→30β(0.59)
	C	5.14	241	0.0001	22α→32α(0.51)
	D	5.93	209	0.003	none[d]
	E	6.10	203	0.005	none[d]
$(CH_3)_2SOH^{\bullet}$,	$X \rightarrow A$	1.63	762	0.0002	22α→23α(0.57)
vertical neutralization	*B*	1.68	737	0.05	22α→24α(0.75)
	C	2.50	496	0.02	22α→25α(0.77)
	D	2.69	461	0.017	22α→26α(0.63)
	E	3.21	387	0.0005	22α→24α(0.71)

[a] Vertical excitation energies. [b] Oscillator strengths. [c] CIS configurations with coefficients >0.5. [d] Highly mixed states.

cal in aqueous solution (358 nm). This difference is in part due to a stabilization of the *B* state by the polar solvent as indicated by the calculated dipole moment of the *B* state (6.5 D) that was substantially larger than that of the ground state (2.5 D). The *B* state can be described as resulting from intramolecular electron transfer from $(CH_3)_2S$ to OH giving rise to a charge-transfer complex, $(CH_3)_2S^{+\bullet}\cdots OH^-$. This interpretation of the *B* state is substantiated by the charge distribution that shows increased positive charge (+0.71) in the DMS moiety and negative charge (–0.71) in the OH group. By comparison, ground state $(CH_3)_2SOH^\bullet$ shows much less polarization, *e.g.* +0.33 charge units in the DMS moiety and –0.33 in the OH group. That the *B* state can be characterized as a $(CH_3)_2S^{+\bullet}\cdots OH^-$ charge-transfer complex is also supported by the calculated atomic spin densities at S (0.75) and O (0.13) that reflect the increased open-shell character of the DMS subunit. The SOMO in the *B* state (Fig. 4, top) shows somewhat larger orbital coefficients at the sulfur atom than does the SOMO in the *X* state (Fig. 4, bottom).

CONCLUSIONS

The present calculations confirm the existence of a bound structure for the $(CH_3)_2SOH^\bullet$ radical and bring energy data obtained at a high level of theory. Vertical electron transfer to the stable gaseous $(CH_3)_2SOH^+$ cation forms $(CH_3)_2SOH^\bullet$ with a highly non-relaxed geometry. The Franck–Condon energy associated with the vertical electron transfer drives unimolecular dissociations to DMS and $OH^\bullet$ and CH_3SOH and $CH_3^\bullet$. The latter dissociation is competitive only when starting from a non-relaxed $(CH_3)_2SOH^\bullet$ that possesses a short S–O bond. Hence, the unimolecular chemistry of $(CH_3)_2SOH^\bullet$ is largely determined by Franck–Condon effects on collisional electron transfer. Electronic excitation in relaxed $(CH_3)_2SOH^\bullet$ shows a dipole-allowed transition to the *B* state that represents a charge-transfer complex of $(CH_3)_2S^{+\bullet}$ and OH^-. The highly polar *B* state is predicted to be stabilized by solvation with polar solvent molecules that results in a bathochromic shift of the absorption wavelength.

Support of this work by the National Science Foundation (Grant CHE-9712750) is gratefully acknowledged. The computations were performed at the Department of Chemistry Computer Facility that received generous funding from the NSF (Grant CHE-9808182). Mr A. Frank and Dr T. Olney kindly provided assistance with data plots.

REFERENCES

1. Tyndall G. S., Ravishankara A. R.: *Int. J. Chem. Kinet.* **1991**, *23*, 483.
2. Turnipseed A. A., Ravishankara A. R. in: *Oceans, Atmosphere and Climate* (G. Restelli and G. Angeletti, Eds), p. 185. Kluwer, Dordrecht 1993.
3. Andrae M. O. in: *The Biogeochemical Cycling of Sulfur and Nitrogen in the Remote Atmosphere* (J. N. Galloway *et al.*, Eds), p. 5. Reiel 1985.
4. Eisele F. L., Bradshaw J. D.: *Anal. Chem.* **1993**, *65*, 927A.
5. Hynes A. J., Wine P. H., Semmes D. H.: *J. Phys. Chem.* **1986**, *90*, 4148.
6. Stickel R. E., Zhao Z., Wine P. H.: *Chem. Phys. Lett.* **1993**, *212*, 312.
7. Hynes A. J., Stoker R. B., Pounds A. J., McKay T., Bradshaw J. D., Nicovich J. M., Wine P. H.: *J. Phys. Chem.* **1995**, *99*, 16967.
8. Tureček F.: *J. Phys. Chem.* **1994**, *98*, 3701.
9. Wine P. H., Kreutter N. M., Gump C. A., Ravishankara A. R.: *J. Phys. Chem.* **1981**, *85*, 2660.
10. Barone S. B., Turnipseed A. A., Ravishankara A. R.: *J. Phys. Chem.* **1996**, *100*, 14694.
11. Turnipseed A. A., Barone S. B., Ravishankara A. R.: *J. Phys. Chem.* **1996**, *100*, 14703.
12. Barnes I., Bastain V., Becker K. H.: *Int. J. Chem. Kinet.* **1988**, *20*, 415.
13. Barnes I., Becker K. H., Patroescu I.: *Geophys. Res. Lett.* **1994**, *21*, 2389.
14. Gu M., Tureček F.: *J. Am. Chem. Soc.* **1992**, *114*, 7146.
15. McKee M. L.: *J. Phys. Chem.* **1993**, *97*, 10971.
16. Merenyi G., Lind J., Engman L.: *J. Phys. Chem.* **1996**, *100*, 8875.
17. Bonifacic M., Mockel H., Bahnemann D., Asmus K.-D.: *J. Chem. Soc., Perkin Trans. 2* **1975**, 675.
18. Chaudri S. A., Gobl M., Freyholy Asmus K.-D.: *J. Am. Chem. Soc.* **1984**, *106*, 5988.
19. Schoneich C., Bobrowski K.: *J. Am. Chem. Soc.* **1993**, *115*, 6538.
20. Gilbert B. C., Hodgeman D. K. C., Norman R. O. C.: *J. Chem. Soc., Perkin Trans. 2* **1973**, 1748.
21. Janata E., Veltwisch D., Asmus K.-D.: *Radiat. Phys. Chem.* **1980**, *16*, 43.
22. Frisch M. J., Trucks G. W., Schlegel H. B., Scuseria G. E., Robb M. A., Cheeseman J. R., Zakrzewski V. G., Montgomery J. A., Jr., Stratmann R. E., Burant J. C., Dapprich S., Millam J. M., Daniels A. D., Kudin K. N., Strain M. C., Farkas O., Tomasi J., Barone V., Cossi M., Cammi R., Mennucci B., Pomelli C., Adamo C., Clifford S., Ochterski J., Petersson G. A., Ayala P. Y., Cui Q., Morokuma K., Malick D. K., Rabuck A. D., Raghavachari K., Foresman J. B., Cioslowski J., Ortiz J. V., Stefanov B. B., Liu G., Liashenko A., Piskorz P., Komaromi I., Gomperts R., Martin R. L., Fox D. J., Keith T., Al-Laham M. A., Peng C. Y., Nanayakkara A., Gonzalez C., Challacombe M., Gill P. M. W., Johnson B., Chen W., Wong M. W., Andres J. L., Gonzalez C., Head-Gordon M., Replogle E. S., Pople J. A.: *Gaussian 98, Revision A.6*. Gaussian, Inc., Pittsburgh (PA) 1998.
23. Parr R. G., Yang W.: *Density Functional Theory of Atoms and Molecules*. Oxford University Press, New York 1989.
24. a) Becke A. D.: *J. Chem. Phys.* **1993**, *98*, 1372; b) Becke A. D.: *J. Chem. Phys.* **1993**, *98*, 5648.
25. Stephens P. J., Devlin F. J., Chablowski C. F., Frisch M. J.: *J. Phys. Chem.* **1994**, *98*, 11623.
26. Frisch M. J., Pople J. A., Binkley J. S.: *J. Chem. Phys.* **1984**, *80*, 3265.
27. Bauschlicher C. W., Partridge H.: *J. Chem. Phys.* **1995**, *103*, 1788.

28. Tureček F.: *J. Phys. Chem. A* **1998**, *102*, 4703.
29. Møller C., Plesset M. S.: *Phys. Rev.* **1934**, *46*, 618.
30. Rauhut G., Pulay R.: *J. Phys. Chem.* **1995**, *99*, 3093.
31. Finley J. W., Stephens P. J.: *J. Mol. Struct. (THEOCHEM)* **1995**, *227*, 357.
32. Wong M. W.: *Chem. Phys. Lett.* **1996**, *256*, 391.
33. Scott A. P., Radom L.: *J. Phys. Chem.* **1996**, *100*, 16502.
34. Tureček F., Cramer C. J.: *J. Am. Chem. Soc.* **1995**, *117*, 12243.
35. McClurg R. B., Flagan R. C., Goddard W. A., III: *J. Chem. Phys.* **1997**, *106*, 6675.
36. East A. L. L., Radom L.: *J. Chem. Phys.* **1997**, *106*, 6655.
37. Dunning T. H., Jr.: *J. Chem. Phys.* **1989**, *90*, 1007.
38. Pople J. A., Head-Gordon M., Raghavachari K.: *J. Chem. Phys.* **1987**, *87*, 5968.
39. Curtiss L. A., Raghavachari K., Pople J. A.: *J. Chem. Phys.* **1993**, *98*, 1293.
40. Curtiss L. A., Raghavachari K., Redfern P. C., Pople J. A.: *J. Chem. Phys.* **1997**, *106*, 1063.
41. Raghavachari K., Stefanov B. B., Curtiss L. A.: *J. Chem. Phys.* **1997**, *106*, 6764.
42. Smith B. J., Radom L.: *J. Phys. Chem.* **1995**, *99*, 6468.
43. Curtiss L. A., Raghavachari K., Pople J. A.: *J. Chem. Phys.* **1995**, *103*, 4192.
44. Tureček F., Polášek M., Frank A. J., Sadílek M.: *J. Am. Chem. Soc.* **2000**, *122*, 2 3 6 1 .
45. Mayer I.: *Adv. Quantum Chem.* **1980**, *12*, 189.
46. Schlegel H. B.: *J. Chem. Phys.* **1986**, *84*, 4530.
47. McWeeny R., Diercksen G.: *J. Chem. Phys.* **1968**, *49*, 4852.
48. Parkinson C. J., Mayer P. M., Radom L.: *J. Chem. Soc., Perkin Trans. 2* **1999**, 2305.
49. Sadílek M., Tureček F.: *J. Phys. Chem.* **1996**, *100*, 9610.
50. Sadílek M., Tureček F.: *J. Phys. Chem.* **1996**, *100*, 15027.
51. Nguyen V. Q., Sadílek M., Frank A. J., Ferrier J. G., Tureček F.: *J. Phys. Chem. A* **1997**, *101*, 3789.
52. Sadílek M., Tureček F.: *Int. J. Mass Spectrom.* **1999**, *185/186/187*, 639.
53. Mallard W. G., Lindstrom P. J. (Eds): *NIST Chemistry Webbook, NIST Standard Reference Database*, No. 69. NIST, Gaithersburg (MD) 1998; http://webbook.nist.gov/chemistry.
54. The enthalpy of formation of OOH in ref.[53] (2.092 kJ mol^{-1}) is a typographical error.
55. Aston J. G., Fritz J. J.: *Thermodynamics and Statistical Thermodynamics*. Wiley, New York 1959.
56. Dunbar R. C.: *J. Chem. Phys.* **1989**, *90*, 7369.
57. Foresman J. B., Head-Gordon M., Pople J. A., Frisch M. J.: *J. Phys. Chem.* **1992**, *96*, 135.